OPEN ACCESS

Absolute frequency measurements of ^{85}RbnF$_{7/2}$ Rydberg states using purely optical detection

New Journal of Physics
The open-access journal for physics

Absolute frequency measurements of ^{85}Rb n $F_{7/2}$ Rydberg states using purely optical detection

L A M Johnson[1,3], H O Majeed[1], B Sanguinetti[1], Th Becker[2] and B T H Varcoe[1]

[1] School of Physics and Astronomy, University of Leeds, Leeds LS2 9JT, UK
[2] Max Planck Institute of Quantum Optics, Hans Kopfermann Strasse 1 85748 Garching, Germany
E-mail: L.A.M.Johnson07@leeds.ac.uk

New Journal of Physics **12** (2010) 063028 (12pp)
Received 16 February 2010
Published 15 June 2010
Online at http://www.njp.org/
doi:10.1088/1367-2630/12/6/063028

Abstract. A three-step laser excitation scheme is used to make absolute frequency measurements of highly excited $nF_{7/2}$ Rydberg states in ^{85}Rb for principal quantum numbers $n = 33$–100. This work demonstrates the first absolute frequency measurements of rubidium Rydberg levels using a purely optical detection scheme. The Rydberg states are excited in a heated Rb vapour cell and Doppler-free signals are detected via purely optical means. All of the frequency measurements are made using a wavemeter that is calibrated against a Global Positioning System (GPS)-disciplined self-referenced optical frequency comb. We find that the measured levels have a very high frequency stability, and are especially robust against electric fields. The apparatus has allowed measurements of the states to an accuracy of 8.0 MHz. The new measurements are analysed by extracting the modified Rydberg–Ritz series parameters.

[3] Author to whom any correspondence should be addressed.

Contents

1. Introduction

The accurate measurement of highly excited Rydberg level energies in alkali atoms plays an important role in improving the accuracy of atomic models [1]. In most Rydberg spectroscopy experiments, atoms are detected via field ionization. However, in this study we use a method of purely optical detection in an ordinary vapour cell, which has been demonstrated in [2]–[5]. A vapour cell is a convenient and straightforward solution for finding Rydberg levels, which could potentially permit rapid advances in Rydberg spectroscopy. This technique presents a method of finding Rydberg states quickly, with a large signal-to-noise ratio and an apparent insensitivity to electric fields [3, 4], which makes it particularly well-suited for studying high ℓ Rydberg states with large polarizabilities. It is therefore important to verify the ability to perform precision spectroscopy in such a setup.

Although there is a large body of work on precision interval and fine structure measurements of the different rubidium Rydberg series [6]–[10], measurements of the absolute energies of these levels are more difficult to carry out, and are therefore mainly limited to the lower ℓ states [11]–[14]. It appears that absolute measurements of the ^{85}Rb nF series have only been made once by Johansson in 1961 [15] for $n = 4$–8. However, as new tools are now available in laser spectroscopy, such as the optical frequency-comb technique, it is interesting to return to such measurements. In this work we wish to demonstrate that precision laser spectroscopy measurements of Rydberg states can be made effectively using purely optical detection with a vapour cell sample.

During the experiment, $n\mathrm{F}_{7/2}$ Rydberg states between $n = 33$–100 were excited in ^{85}Rb using a three-step laser excitation scheme identical to that outlined in [4, 14]. The three-step level system, shown in figure 1, consists of a 780.24 nm transition $5\mathrm{S}_{1/2}$ $F = 3$ to $5\mathrm{P}_{3/2}$ $F = 4$, a 775.98 nm transition $5\mathrm{P}_{3/2}$ $F = 4$ to $5\mathrm{D}_{5/2}$ $F = 5$ and finally a 1260 nm transition $5\mathrm{D}_{5/2}$ to $n\mathrm{F}_{7/2}$.

To observe excitations to Rydberg states, the first two-step lasers are fixed at their respective transition frequencies and the absorption of the 780 nm laser is monitored while the 1260 nm laser is swept across the transition of interest. This technique involves the quantum amplification effect; due to the large differences in the decay lifetimes of the three excited states of the system, the excitation of a single atom by the third step laser will hinder many absorption–emission cycles on the second step transition. This in turn will hinder a large amount of cycles on the strong first step cycling transition, which can cause a measurable decrease in

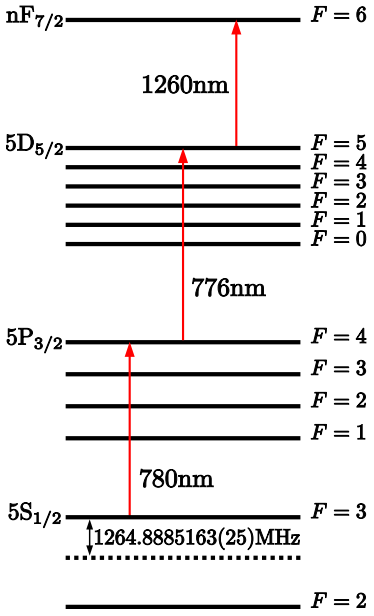

Figure 1. The three-step level scheme used to excite ^{85}Rb nF$_{7/2}$ Rydberg states in this experiment.

the first step absorption. Even for Rydberg atoms confined in a room temperature vapour cell, with the associated limitations of interaction time and interatomic collisions, this amplification factor can be large enough to observe significant changes in absorption [4].

Laser excitation is carried out using σ^+ polarized light on all three steps. Optical pumping on the strong first step transition, along with dipole selection rules, ensures the second step laser only excites to the $m_F = 5$ sublevel of the 5D$_{5/2}$ $F = 5$ hyperfine state and the third step laser only excites a single transition, the 5D$_{5/2}$ $F = 5$ to nF$_{7/2}$ $F = 6$. Having a well-defined pathway to the Rydberg states is important because of the relatively small $\sim$10 MHz hyperfine splitting of the 5D$_{5/2}$ level [16]. Successful optical selection in this scheme was previously demonstrated by one of our co-authors in [4].

2. Apparatus

In the experimental setup, shown in figure 2, all three steps are excited using commercial tunable external cavity diode lasers and associated electronics. The third step laser is broadly tunable across a range of 110 nm using a precision stepper motor; this allows a large range of nF states to be accessed. The first and third step lasers are superimposed and co-propagate through an uncoated rubidium vapour cell of length 80 mm. The second step laser travels through the same cell; it counter-propagates and overlaps with the first and third step lasers. Absorption of the first step laser is monitored using a conventional photodiode as the third step laser is swept across the 5D$_{5/2}$ to nF$_{7/2}$ transition of interest. Removal of the first step laser from the other two laser paths is carried out using a polarizing beam splitter. The first two steps are circularly polarized using quarter wave plates, and the third step laser is circularly polarized using a broadband Fresnel rhomb. All three lasers are focused to a beam waist of $\sim$100 μm inside the cell, which increases the available third step laser power density, allowing an interaction time of about 1 μs. The first

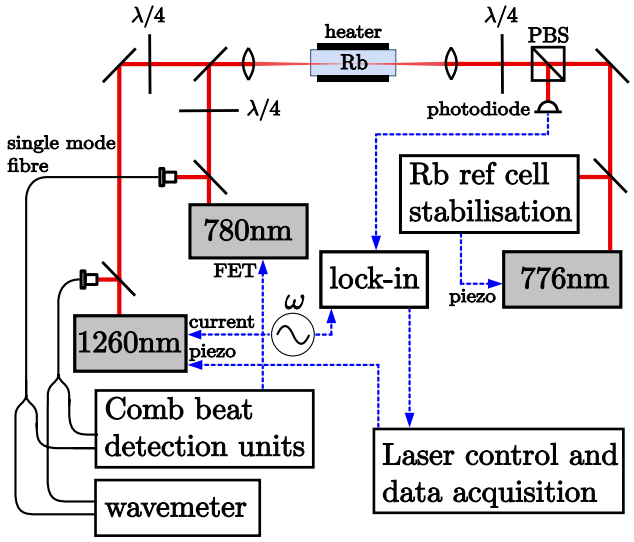

Figure 2. Experimental setup used for measuring Rydberg state frequencies. The first step is phase locked to a self-referenced optical frequency comb and the second step is frequency locked using a separate rubidium reference cell. The first and third step laser light is transported to the comb and wavemeter using single-mode optical fibres.

and second step transitions are driven just below saturation intensity. We were unable to saturate the third step with the 3 mW of available laser power. The laser powers are chosen to give the largest Rydberg excitation rate, with minimal power broadening. The vapour cell is heated to a temperature of 60 °C to increase the atomic density in the cell and to therefore enhance the first step absorption.

In this experiment the first step laser Doppler selects those atoms that take part in subsequent excitations; therefore, it is important that the first step frequency is well known and well stabilized. Hence we stabilize this laser to a self-referenced frequency comb, by phase locking the beat note between the laser and a comb line to a stable direct digital synthesizer. The frequency comb repetition rate is adjusted such that the laser frequency is stabilized to 384 229 242.8 MHz, corresponding to the first step transition frequency from [17]. All locking circuits are referenced to a GPS-disciplined rubidium frequency standard. The comb system allows laser frequencies to be measured with an absolute accuracy of 10^{-11}. Fast feedback for the offset lock is supplied using a field-effect transistor connected to the laser diode. The stability of the first step lock was measured as less than 100 Hz over all time scales relevant to this experiment. However, the absolute accuracy is limited to the measurement uncertainty of 750 kHz from Barwood *et al* [17], who observed anomalous offsets on this particular transition, which limits its accuracy as a standard.

Before adding the third step laser to the system, we verified that efficient optical pumping was occurring on the first step transition by scanning the second step laser across the $5D_{5/2}$ manifold, with the first step laser locked. The first step laser selects only zero-velocity atoms, and therefore the second step laser scan showed a single and symmetric Doppler-free peak in the first step absorption. This single peak, with a full width at half maximum (FWHM) of 11.5 MHz, corresponds to the reduced absorption of the first step laser as the second step laser excites

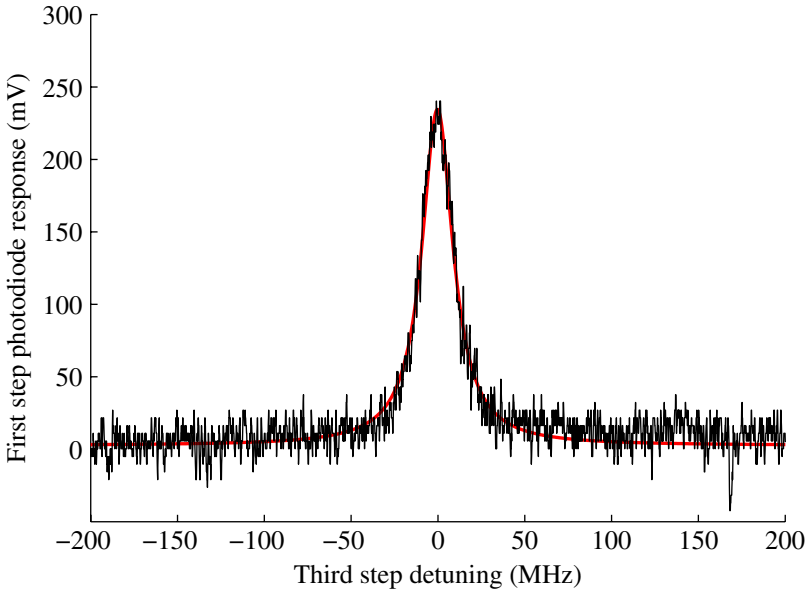

Figure 3. A scan of the third step laser across the $33F_{7/2}$ Rydberg state from an oscilloscope. The vertical axis is the first step transmitted intensity from the photodiode; an offset of 10.1 V has been subtracted for convenience. The frequency axis was calibrated with a Fabry–Pérot resonator at 1268 nm. The fitted curve is a Lorentzian with an FWHM of 20 MHz.

the $5P_{3/2}$ $F = 4$ to $5D_{5/2}$ $F = 5$ transition, singled out by the dipole-selection rules. To confirm this we measured the absolute frequency of this transition using our frequency comb and added it to the first step locked frequency to get 770 570 284(1) MHz. This agrees with 770 570 284 734(8) kHz from [16], obtained from two-photon spectroscopy. This therefore demonstrates that the excitation pathway of the first two steps is well understood. This scheme is also used to stabilize the second step laser with a separate room temperature vapour cell. By adding a small frequency modulation to the second step laser, and monitoring the first step absorption via a lock-in amplifier, an error signal is extracted. Using our frequency comb we verified that this second step frequency lock was repeatable to an absolute accuracy of 1 MHz on a daily basis.

We found that it is possible to detect lower n states with a very good signal-to-noise ratio. Therefore, to verify the line shape of the detected signals, the photodiode was monitored directly on an oscilloscope during a fast scan across the $5D_{5/2}$ to $33F_{7/2}$ transition. The trace is displayed in figure 3. The scan was carried out in 10 ms and the frequency axis was calibrated using a Fabry–Pérot resonator. The data fit a Lorentzian function with a linewidth of 20 MHz. This linewidth prevents the $nF_{7/2}$ and $nF_{5/2}$ fine structure splitting from being resolved, which for $n = 33$ to 100 is 4.35 MHz to 0.16 MHz, respectively [9]. However, the use of σ^+ light on the third step ensures that only the $nF_{7/2}$ level is excited in this case. This is confirmed by the symmetry of the trace in figure 3, and the absence of any visible effect of the $nF_{5/2}$ level. Even if there is a complete redistribution of the m_F levels in the $5D_{5/2}$ $F = 5$ state due to the Earth's magnetic field, we expect the transition to the $nF_{5/2}$ level to contribute at most 5% to the signal, which can be calculated from the relevant $6j$ symbols.

To improve the detection sensitivity of third step transitions, a frequency modulation is added to the third step laser via the injection current, with a modulation amplitude of 15 MHz

and a frequency of 6 kHz. Detection of the first step absorption is carried out at the first harmonic using a lock-in amplifier with a time constant of 1 s. The free-running third step laser is scanned by applying a linear voltage ramp to the laser piezo using computer software and a digital to analogue converter interface. The free-running laser stability was measured as less than 1 MHz over 1 s, which is sufficient to carry out slow scans across the Rydberg transitions. As the third step laser is scanned, its absolute frequency is monitored using a WS7 High Finesse wavemeter. The wavemeter readings are recorded simultaneously using the same computer software.

We used our frequency comb to check the wavemeter's accuracy and stability across the range of third step laser wavelengths used in this experiment. This was carried out by stabilizing the third step laser to the comb at arbitrary frequencies across the 1254–1268 nm range, where there was a coincident comb line, and measuring its frequency with the wavemeter. We found that the wavemeter's stability stayed below 2 MHz for times of $\sim$1000 s. We also found that the wavemeter was able to maintain a day-to-day absolute accuracy of 6.2 MHz across this range, when regularly calibrated at 780 nm. Therefore, throughout this experiment the wavemeter is calibrated every 30 min to the comb-locked first step laser, to supply a direct frequency link with the comb.

3. Results

The third step transition absolute frequencies were collected for $n = 33$–50 in intervals of one, and from $n = 50$–100 in larger intervals of five. Fitting to the transition data was done using a Wahlquist first derivative function [18]. The function is given by

$$f(H_\delta) = \frac{H_\delta}{|H_\delta|}\left(\frac{2}{H_\omega}\right)^2 \frac{\sqrt{2\gamma - u}}{2\sqrt{u-2}(u-\gamma)}, \tag{1}$$

where $\gamma = 1 + \beta^2 + \alpha^2$, $u = \gamma + \sqrt{\gamma^2 - 4\alpha^2}$, $\alpha = H_\delta / H_\omega$ and $\beta = (\frac{1}{2} H_{1/2}/H_\omega)$. $H_{1/2}$, H_ω and H_δ are the FWHM, modulation amplitude and frequency detuning, respectively. Figure 4 shows a typical scan across a Rydberg transition with the fitted profile from (1).

Ten traces were taken for each state in order to understand the repeatability of the measurements. It was found that on average the standard deviation of each set of ten scans was 2 MHz with an accuracy limited by the short-term drift of the wavemeter during the time taken to collect each set. The mean transition frequencies of the third step are summarized in the second column of table 1. The third column of this table displays the total $5S_{1/2}$ to $nF_{7/2}$ frequency, measured from the centre of mass of the $5S_{1/2}$ ground states. These values were calculated by adding a constant value of 770 571 549.6 MHz to the third step transition frequencies in column two; this frequency was computed from [16] and [19].

Rydberg atom interactions, for example the dipole–dipole interaction, scale strongly with inter-atomic spacing [20]. It was therefore important to eliminate any pressure-dependent shifts. We estimate an average inter-atomic Rydberg atom spacing of $\sim 10\,\mu$m, which is where we expect to see observable shifts of a few MHz for the $100F_{7/2}$ state [20]. As well as causing a broadening, increased power of any of the three lasers could also cause systematic shifts of Rydberg signals. We expect both Rydberg atom density and m_F state selection efficiency to have some dependence on laser power, both of which could result in a peak pulling. There could also be a contribution from the light shift [16]. To target systematics from pressure and laser power, we took measurements of the $33F_{7/2}$ and $100F_{7/2}$ transitions with a range of cell temperatures from 20 to 65 °C and a range of first, second and third step laser powers, respectively. In all cases

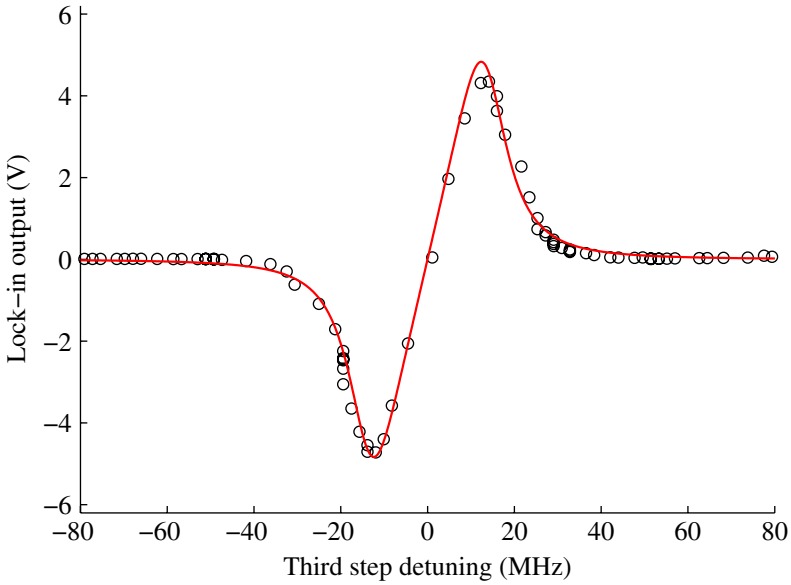

Figure 4. A typical scan of the third step laser across the $33F_{7/2}$ Rydberg state. The plot displays the demodulated first step absorption from the lock-in amplifier against the absolute frequency of the third step laser from the WS7 wavemeter.

we were unable to detect any repeatable trends in the transition frequencies. Therefore, potential offsets from both temperature- and power-dependent shifts were not added as corrections, but instead the spread of measurements was used to estimate the maximum possible error in each individual case.

Using a fluxgate magnetometer, the magnitude of stray magnetic fields was measured along the axis of the vapour cell as $<20\,\mu$T. The Zeeman shift of the $n\mathrm{F}_{7/2}$ $F = 6$ $m_F = 6$ level is $0.06\,\mathrm{MHz}\,\mu\mathrm{T}^{-1}$, which gives a Zeeman shift of <1.1 MHz. However, because of the four-level nature of the excitation we actually expect Zeeman shifts of the transitions to be equal to the difference in Zeeman shifts between subsequent levels of the excitation scheme, in this case $14\,\mathrm{kHz}\,\mu\mathrm{T}^{-1}$ for each of the three steps. We therefore estimate a maximum Zeeman shift of 840 kHz. To check for this shift, measurements of the $33F_{7/2}$ state were made with both $\sigma_+\sigma_+\sigma_+$ and $\sigma_-\sigma_-\sigma_-$ polarized light on the three excitation steps, respectively. Equal and opposite Zeeman shifts are expected for these two cases. We were unable to detect any difference within the short-term drifts of the wavemeter, and therefore we assume that the contribution to the total uncertainty from this effect is negligible. As an additional test of the optical arrangement, and the magnetic field sensitivity, we applied magnetic fields of $100\,\mu$T along the axis of the cell. In this case we were able to measure shifts of the Rydberg signals of up to 5 MHz.

We also checked for errors from hysteresis and time delays in the data acquisition process by scanning the third step laser across the same transition in opposing directions. We found no difference in these two measurements. The summarized error estimates are displayed in table 2. The wavemeter calibration is a source of random error and all other uncertainties are systematic in nature. The errors add in quadrature to give a total error of 8.0 MHz.

Rydberg nF states are highly polarizable in external electric fields, with polarizabilities scaling as n^7 [21]. However, in [3] and [4] no dc Stark shifts were observed when detecting Rydberg atoms in a vapour cell, for electric fields of up to $100\,\mathrm{V\,cm}^{-1}$. This makes a cell

Table 1. Third step transition frequencies ν_3 and total $5S_{1/2}$ to $nF_{7/2}$ transition frequencies E_n for $n = 33$–100. The total frequencies are measured from the centre of mass of the two $5S_{1/2}$ hyperfine ground states. The total accumulated error on all frequencies is 8.0 MHz.

n	ν_3 (MHz)	E_n (MHz)
33	236 429 214	1007 000 764
34	236 604 549	1007 176 099
35	236 765 078	1007 336 627
36	236 912 402	1007 483 952
37	237 047 954	1007 619 503
38	237 172 932	1007 744 481
39	237 288 417	1007 859 967
40	237 395 343	1007 966 892
41	237 494 542	1008 066 092
42	237 586 734	1008 158 283
43	237 672 570	1008 244 119
44	237 752 610	1008 324 159
45	237 827 379	1008 398 929
46	237 897 325	1008 468 875
47	237 962 850	1008 534 399
48	238 024 325	1008 595 874
49	238 082 056	1008 653 605
50	238 136 367	1008 707 917
55	238 364 972	1008 936 522
60	238 538 826	1009 110 376
65	238 674 124	1009 245 673
70	238 781 461	1009 353 011
75	238 868 053	1009 439 602
80	238 938 927	1009 510 477
85	238 997 658	1009 569 208
90	239 046 866	1009 618 416
95	239 088 516	1009 660 066
100	239 124 074	1009 695 624

an excellent spectroscopic sample, by eliminating a potential systematic. To check that this experiment was also insensitive to electric fields, we applied electric fields of up to 30 V cm^{-1} across the vapour cell and checked for frequency shifts of both the $33F_{7/2}$ and $100F_{7/2}$ transitions. In each case there was no measurable deviation.

4. Analysis

Rydberg level energies are very well described by the Rydberg formula

$$E_n = E_\mathrm{i} - \frac{R_X}{[n - \delta(n)]^2} = E_\mathrm{i} - \frac{R_X}{n^{*2}}, \tag{2}$$

Table 2. Estimated errors.

Type	Source	Error
Random	Wavemeter calibration	6.2 MHz
Systematic	First step frequency	750 kHz
	Second step frequency	1.0 MHz
	Pressure shifts	2.7 MHz
	Power-dependent shifts	4.0 MHz
	Total	8.0 MHz

where E_i is the ionization energy, E_n is the excitation energy from the ground state to a state with principal quantum number n, R_X is the Rydberg constant for the atom of interest, $\delta(n)$ is the quantum defect and n^* is the effective quantum number. The quantum defect can also be written as a Ritz expansion

$$\delta(n) = \delta_0 + \delta_2 t_n + \delta_4 t_n^2 + \cdots, \tag{3}$$

where

$$t_n = \frac{1}{[n - \delta(n)]^2} = \frac{E_\mathrm{i} - E_n}{R_X}. \tag{4}$$

The data from this experiment were analysed using three different fitting methods. The first two methods follow the same theme as [22], while the third method is a consistency check of the data with previous work. These methods are outlined in sections 4.1, 4.2 and 4.3. To aid in the analysis, five values of E_n for $n = 4$–8 were added to the data set from [15]. Weighted fitting was important to take account of the larger uncertainties on these older measurements. Throughout the analysis the Rydberg constant for rubidium 85 was taken as $R_\mathrm{Rb} = 10\,973\,660.672\,249 \times c$ from [14].

4.1. Method 1

In method 1 the energy levels E_n were fitted using a least squares fitting procedure to the formula

$$E_n = E_\mathrm{i} - \frac{R_\mathrm{Rb}}{\left[n - \delta_0 - \delta_2 t_n - \delta_4 t_n^2 - \cdots\right]^2}. \tag{5}$$

The fit algorithm balanced both sides of (5) to find the optimum parameters for $E_\mathrm{i}, \delta_0, \delta_2, \delta_4, \ldots$. The results from this fit are displayed in table 3 and the residuals are shown in figure 5. Drake and Swainson [1] describe in great detail how the series parameters extracted from this type of fit can explain physical properties of the Rydberg atom, such as core polarization.

4.2. Method 2

To remove the recursive nature of (3), it is common to make the approximation

$$t_n \approx \frac{1}{(n - \delta_0)^2}, \tag{6}$$

Table 3. Fit parameters from the method 1, 2 and 3 fitting routines. The method 1 fit gives the series parameters δ_0, δ_2 and δ_4; see [1]. The method 2 and 3 fits, and [9], give the equivalent series parameters δ_0, a and b; see [22]. Uncertainties are statistically derived from the fitting. The errors on the E_i values include possible systematic contributions outlined in table 2. The parameters from [9] are shown for comparison with the method 3 results.

	E_i (MHz)	δ_0	δ_2,a	δ_4,b
Method 1	1010 024 719(8)	0.016 473(14)	−0.0783(7)	0.028(7)
Method 2	1010 024 719(8)	0.016 473(14)	−0.0784(7)	0.032(7)
Method 3	1010 024 717(8)	0.016 40(8)	0.00(9)	–
Jianing *et al* [9]	–	0.016 5437(7)	−0.086(7)	–

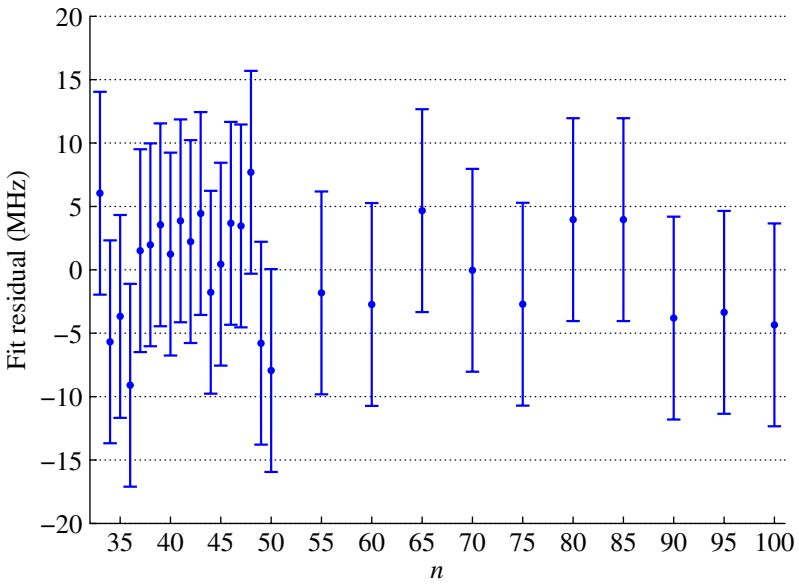

Figure 5. Residuals for the $n = 33$–100 states from the method 1 fitting routine. The error bars show the total accumulated error on each data point of 8.0 MHz.

which when substituted into (5) gives a Rydberg–Ritz expression that can be evaluated with greater simplicity [22]:

$$E_n = E_i - \frac{R_{Rb}}{[n - \delta_0 - \frac{a}{(n-\delta_0)^2} - \frac{b}{(n-\delta_0)^4} - \cdots]^2}. \tag{7}$$

The method 2 fit involved a direct least squares fit of (7) to the energy levels E_n. The results from this fit are displayed in table 3 where the a and b parameters are placed underneath the equivalent δ_2 and δ_4 parameters from the method 1 fit. It can be seen that the values of E_i and the series parameters extracted from the first two fitting methods agree to well within the uncertainties. The value of E_i from this work also lies within 2σ of the previous value from [14]. An analysis of the residuals shown in figure 5, from the method 1 fit, shows that the points are scattered around a mean of zero with a standard deviation of 4.4 MHz. The states were measured

across several days and therefore this spread comes mainly from the long-term accuracy of the wavemeter.

The Rydberg–Ritz formula in (7) has the significant advantage that it allows any energy level E_n to be calculated with knowledge only of the principal quantum number n. In this manner, (7) can be used with the relevant parameters in table 3 to predict the absolute energies of other rubidium $n\mathrm{F}_{7/2}$ states outside the range of this experiment.

4.3. Method 3

As a consistency check of these data, we compared the Ritz series parameters extracted from our absolute measurements with those from the most recent relative interval measurements [9]. For this fit we used an abridged version of (7),

$$E_n = E_\mathrm{i} - \frac{R_\mathrm{Rb}}{[n - \delta_0 - \frac{a}{(n-\delta_0)^2}]^2}. \tag{8}$$

This is the equivalent function that was used for fitting in [9] and is an accurate approximation for $n \geqslant 20$. For this reason we restricted this fit to the $n \geqslant 33$ levels. The parameters from this fitting method are shown in table 3 with the values from [9]. The a parameter is placed underneath the equivalent δ_2 parameter from the method 1 fit.

It can be seen that the δ_0 and a parameters from this fit agree at the 2σ level with those from the previous work [9]. Our parameters are extracted from absolute measurements. Therefore, one does not expect as high a precision as from interval measurements; however, absolute measurements do have the advantage that the ionization energy E_i can also be extracted. The larger errors on the series parameters from this fit, as compared to the method 1 and 2 fits, arise because of the absence of lower n states. This makes extracting higher order series parameters more difficult. For example, in (7), for lower n states the parameters δ_0 and a make a bigger contribution than for higher n states, where E_n becomes dominated by E_i. As displayed in table 3, the addition of the lower n states from [15] greatly aided in the reliable extraction of the higher order parameters in the method 1 and 2 fitting routines.

5. Conclusion

We have presented absolute frequency measurements of $n\mathrm{F}_{7/2}$ Rydberg states in rubidium 85 to an accuracy of 8.0 MHz. This is a factor 40 improvement over previous measurements of the $n = 4$–8 $n\mathrm{F}_{7/2}$ states [15], and gives measurements for a range of $n\mathrm{F}_{7/2}$ states between $n = 33$–100 for the first time. The Rydberg–Ritz series parameters that have been extracted from this work allow absolute energies of $n\mathrm{F}_{7/2}$ states with higher or lower principal quantum number n to be predicted with comparable accuracy. Our new measurements also show consistency with the results from recent microwave spectroscopy experiments [9]. This work demonstrates that methods of Rydberg spectroscopy involving purely optical detection can be used very effectively to carry out precision measurements of Rydberg states in a simple way, and with extraordinary robustness to dc stark shifts. Not only is the setup simple to construct and maintain but it is easier to use than beam experiments, and Rydberg signals can be monitored in real time on an oscilloscope. We believe that this experiment could be readily adapted to study other alkali metal atoms and could even be used to study unusual features such as Rydberg–Rydberg interactions and molecular states.

References

[1] Drake G W F and Swainson R A 1991 Quantum defects and the 1/n dependence of Rydberg energies: second-order polarization effects *Phys. Rev.* A **44** 5448–59

[2] Brandenberger J R, Regal C A, Jung R O and Yakes M C 2002 Fine-structure splittings in ^2f states of rubidium via three-step laser spectroscopy *Phys. Rev.* A **65** 042510

[3] Mohapatra A K, Jackson T R and Adams C S 2007 Coherent optical detection of highly excited Rydberg states using electromagnetically induced transparency *Phys. Rev. Lett.* **98** 113003

[4] Thoumany P, Germann Th, Hänsch T, Stania G, Urbonas L and Becker Th 2009 Spectroscopy of rubidium Rydberg states with three diode lasers *J. Mod. Opt.* **56** 2055–60

[5] Kübler H, Shaffer J P, Baluktsian T, Löw R and Pfau T 2010 Coherent excitation of Rydberg atoms in micrometre-sized atomic vapour cells *Nat. Photonics* **4** 112–6

[6] Harvey K C and Stoicheff B P 1977 Fine structure of the n^2D series in rubidium near the ionization limit *Phys. Rev. Lett.* **38** 537–40

[7] Meschede D 1987 Centimeter-wave spectroscopy of highly excited rubidium atoms *J. Opt. Soc. Am.* B **4** 413–9

[8] Wenhui L, Mourachko I, Noel M W and Gallagher T F 2003 Millimeter-wave spectroscopy of cold Rb Rydberg atoms in a magneto-optical trap: quantum defects of the ns, np, and nd series *Phys. Rev.* A **67** 052502

[9] Jianing H, Yasir J, Norum D V L, Tanner Paul J and Gallagher T F 2006 Rb nf quantum defects from millimeter-wave spectroscopy of cold ^{85}Rb Rydberg atoms *Phys. Rev.* A **74** 054502

[10] Afrousheh K, Bohlouli-Zanjani P, Petrus J A and Martin J D D 2006 Determination of the ^{85}Rb ng-series quantum defect by electric-field-induced resonant energy transfer between cold Rydberg atoms *Phys. Rev.* A **74** 062712

[11] Lee S A, Helmcke J, Hall J L and Stoicheff B P 1978 Doppler-free two-photon transitions to Rydberg levels: convenient, useful, and precise reference wavelengths for dye lasers *Opt. Lett.* **3** 141–3

[12] Stoicheff B P and Weinberger E 1979 Doppler-free two-photon absorption spectrum of rubidium *Can. J. Phys.* **57** 2143–54

[13] Lorenzen C J and Niemax K 1983 Quantum defects of the $n^2P_{1/2,3/2}$ levels in ^{39}K I and ^{85}Rb I *Phys. Scr.* **27** 300–5

[14] Sanguinetti B, Majeed H O, Jones M L and Varcoe B T H 2009 Precision measurements of quantum defects in the nP$_{3/2}$ Rydberg states of ^{85}Rb *J. Phys. B: At. Mol. Opt. Phys.* **42** 165004

[15] Johansson I 1961 Spectra of the alkali metals in the lead-sulphide region *Ark. Fys.* **20** 135–46

[16] Nez F, Biraben F, Felder R and Millerioux Y 1993 Optical frequency determination of the hyperfine components of the 5S$_{1/2}$–5D$_{3/2}$ two-photon transitions in rubidium *Opt. Comm.* **102** 432–8

[17] Barwood G P, Gill P and Rowley W R C 1991 Frequency measurements on optically narrowed Rb-stabilised laser diodes at 780 nm and 795 nm *Appl. Phys.* B **53** 142–7

[18] Wahlquist H 1961 Modulation broadening of unsaturated Lorentzian lines *J. Chem. Phys.* **35** 1708–10

[19] Arimondo E, Inguscio M and Violino P 1977 Experimental determinations of the hyperfine structure in the alkali atoms *Rev. Mod. Phys.* **49** 31–75

[20] Saffman M, Walker T G and Molmer K 2010 Quantum information with Rydberg atoms arXiv:0909.4777v2 [quant-ph]

[21] Gallagher T F 1988 Rydberg atoms *Rep. Prog. Phys.* **51** 143–88

[22] Martin W C 1980 Series formulas for the spectrum of atomic sodium (Na I) *J. Opt. Soc. Am.* **70** 784–8